Title: Water Transport Regulates Nucleus Volume, Cell Density, Young's Modulus, and E-

cadherin expression in Tumor Spheroids

AUTHORS: Christina Conrad¹, Jessica Conway¹, William J. Polacheck², Imran Rizvi² and

Giuliano Scarcelli¹

AFFILIATIONS:

¹ Fischell Department of Bioengineering, University of Maryland, College Park, MD

² Joint Department of Biomedical Engineering, University of North Carolina at Chapel Hill and

North Carolina State University, Chapel Hill, NC

CORRESPONDENCE:

Dr. Giuliano Scarcelli

4228 A. James Clark Hall

Fischell Department of Bioengineering

University of Maryland

College Park, MD, 20742

USA

Tel: 1-301-314-1689

Fax: 1-301-405-9953

Email: scarc@umd.edu

1

Abstract: Cell volume is maintained by the balance of water and solutes across the cell membrane

and plays an important role in mechanics and biochemical signaling in cells. Here, we assess the

relationship between cell volume, mechanical properties, and E-cadherin expression in three-

dimensional cultures for ovarian cancer. To determine the effect of water transport in multi-cellular

tumors, ovarian cancer spheroids were subjected to hypotonic and hypertonic shock using water

and sucrose mixtures, respectively. Increased osmolality resulted in decreased nucleus volume,

increased Young's modulus, and increased tumor cell density in ovarian cancer spheroids. Next,

we looked at the reversibility of mechanics and morphology after 5 minutes of osmotic shock and

found that spheroids had a robust ability to return to their original state. Finally, we quantified the

size of E-cadherin clusters at cell-cell junctions and observed a significant increase in aggregate

size following 30 minutes of hypertonic and hypotonic osmotic shocks. Yet, these effects were not

apparent after 5 minutes of osmotic shock, illustrating a temporal difference between E-cadherin

regulation and the immediate mechanical and morphology changes. Still, the osmotically induced

E-cadherin aggregates which formed at the 30-minute timepoint was reversible when spheroids

were replenished with isotonic medium. Altogether, this work demonstrated an important role of

osmolality in transforming mechanical, morphology, and molecular states.

Keywords: Cell volume, osmolality, mechanics, cancer, E-cadherin

2

I. Introduction

Water volume regulation plays an important role in numerous processes across length scales, from organisms to cells. (1) Approximately 50 to 75% of the human body is composed of water, with 70 to 75% being stored in cells and the remaining amount in plasma and interstitial spaces. (2) On an organ system-level, the kidneys are responsible for maintaining a balance between solutes and water in serum. The average serum osmolality in humans is 286 mOsm/kg H₂O, but fluctuates depending on water and nutrient intake. (3) In the case of dehydration, for instance, the concentration of electrolytes in the blood rises. (3) On a cellular system-level, osmoregulation is achieved by the exchange of ions (e.g. Na⁺, K⁺ and Cl⁻), organic osmolytes (e.g. sugars, polyols, amino acids, methylamines, and urea), and water to maintain an equal amount of solutes on the inside and outside of cells. (4–7) Accordingly, osmosis drives water flow from a low solute concentration to a high solute concentration. (2) The mobility of water across the lipid bilayer of the cell membrane and into the cytoplasm occurs, in part, by transmembrane passive diffusion through the lipid matrix and also via facilitated diffusion using aquaporins, transmembrane proteins that facilitate water flow, and other membrane proteins, such as glucose transporters. (2, 8-10) Water volume into the nucleus is further altered by passive diffusion through nuclear pore complexes. (11, 12) Whole cell and nucleus volume impact a variety of processes including cell cycle, energy metabolism, DNA repair, migration, proliferation, and differentiation. (13–18) Specifically in cancer, changes in whole cell and nucleus volume have been linked to behaviors such as metastasis, proliferation, and angiogenesis. (19–21) Furthermore, an overexpression of aquaporin transmembrane proteins has been found in several cancer types including lung, breast, ovarian, and prostate. (13, 20, 22–24)

Cell volume is influenced by both the physical environment, for example substrate stiffness (25), or fluid properties like osmolality. (26, 27) Pathologies such as diabetes, sick-cell anemia, and cirrhosis are examples of situations where disruptions in osmotic balances may occur. (28, 29) For instance, hyperosmolar hyperglycemic syndrome (HHS) is a complication that occurs in severe diabetes mellitus, where serum osmolality rises over 320 mOsm/kg H₂O. (30) In the context of cancer, conditions such as hyponatremia (< 130 mEq/L serum sodium levels or < 280 mOsm/kg H₂O serum osmolality) (31, 32) or syndrome of inappropriate secretion of anti-diuretic hormone (SIADH), where excess fluid is retained, can occur in the tumor microenvironment. (29, 33) Specifically in ovarian cancer, an osmotic imbalance may be present due to elevation of fluid levels in the peritoneal cavity (ascites). (34, 35)

In this work, we sought to understand how mechanical properties, nucleus volume, and cell-cell adhesions of multi-cellular 3D ovarian cancer spheroids responded to changes in osmotic conditions. Here, we characterized changes in nucleus volume, density, and Young's modulus in 3D tumor spheroids following stimulation with hypo- and hyper-osmotic shocks. We chose to analyze nucleus volume due to the technical advantage of isolating nuclear volume in a 3D structure using confocal microscopy with nuclear dyes and since previous work has shown that eukaryotic cell volume and nucleus volume scale together at a constant ratio. (26) We also investigated whether water regulation influenced the expression of E-cadherin, an adhesion molecule that binds with cytoplasmic catenins (e.g. p120-catenin, α - catenin, β -catenin) to form adhesive plaques between neighboring cells. (36) Given that mechanics of the surrounding microenvironment can alter E-cadherin expression and localization (37, 38), and osmolality influences cell mechanics (26), there is reason to believe that E-cadherin expression may have ties to volume regulatory mechanisms. Finally, since dynamic phenotypic changes are relevant

throughout the metastatic cascade, (39) we determined whether the morphological, mechanical, and molecular effects induced by osmotic stress were reversible.

I. Materials and Methods

A. Cell Culture

Epithelial ovarian cancer cells (NIH: OVCAR5) were grown using standard procedures. Cells were cultured using RPMI 1640 Medium (Gibco®, #11835030) supplemented with 10% Fetal Bovine Serum (FBS) and 1% Penicillin-Streptomycin. Cells were stored at 37°C and passaged regularly (every 3-5 days).

B. Spheroid Formation

Spheroids were formed using a CorningTM 96-Well, Ultra-Low Binding, U-Shaped-Bottom Microplate (CorningTM #4515). Cells were diluted to a concentration of 15,000 cells/mL and transferred to an MTC-Bio 25mL Reagent Reservoir (Pipette.com, #P8025-1S). 100 μL (approximately 1500 cells) were added to each well the low attachment plate using a Rainin Pipet-LiteTM 12 channel manual pipette (Pipette.com, #L12-200R). Cells were incubated overnight at 37°C to allow for spheroids formation.

C. Polyacrylamide Gels

Polyacrylamide gels were fabricated using a previously established protocol. [33], [34] First, a cotton swab was used to treat the bottom of an 18 mm circular glass coverslip (Electron Microscopy Slides, #72229-01) with 0.1 M NaOH. 200 µl of 3-Cover glasses were coated with Aminopropyltrimethoxysilane (APTMS) for 3 minutes and subsequently washed thoroughly with dH2O. 400 µl of 0.5% glutaraldehyde was added to the cover glasses for 30 min followed by washing with dH2O. Top coverslips were coated with RainX on one side with a cotton swab for 5

minutes and washed with dH2O. Gels with a 1.1 kPa shear modulus were made by combining 94 μl of acrylamide (AA), 15 μl of N,N'-methylene-bis-acrylamide (bis), and 391 μl of phosphate buffered saline (PBS). 1.5 µl of Tetramethylethylenediamine (TEMED) and 5 µl of 10% by weight Ammonium Persulfate (APS) was added to the AA/bis/PBS solution to catalyze polymerization. Solutions were mixed with a 1 mL pipettor set to 400 µl to avoid air bubbles. 20 µl of the solution was pipetted onto each 18 mm diameter glass coverslip. The RainX coated glass coverslip was sandwiched on top of the gel and let sit for 15 minutes to allow the gel to solidify. PBS was added to each gel for another 15 minutes. The top coverslip was then removed using a razor blade and tweezers. 200 µL of 1mg/mL solution of Sulfo-SANPAH in 50mM HEPES and 0.25% DMSO was added to the dishes and placed under a UV lamp for 6 minutes to enable crosslinking. Gels were washed with 50 mM of HEPES. The crosslinking process was performed twice. At the end of the crosslinking, gels were washed 3 times with 50 mM HEPES. Gels were then coated with 1 mL of a Rat Tail Collagen Coating Solution (50 μg/ml, Sigma Aldrich, #122-20). Gels were stored overnight at 4 °C in a 35 mm FluoroDish Cell Culture Dish (World Precision Instruments, #FD35-100).

D. Transfer of Spheroids

Collagen coated polyacrylamide gels were washed three times with PBS. A Rainin Pipet-LiteTM 12 channel manual pipettor set at 50 µl was used to move spheroids to an MTC-Bio 25mL Reagent Reservoir. Then, 2 mL of medium and spheroids was transferred to each collagen-coated gel.

E. Osmotic Shock

Hypotonic shocks were performed by mixing medium with dH₂O at ratios of 1:3 and 1:1. Hypertonic shocks were performed with 500 mM and 1000 mM sucrose added to medium. Osmolality of solutions were measured with an Advanced® Micro-Osmometer Model 3300 using freezing point depression. *Recovery:* For nucleus volume, density, and Young's modulus recovery experiments, hyper/hypo-osmotic shocks were performed for 5 or 30 minutes, followed by restoration with isotonic medium for the same duration as the osmotic shock.

F. Nucleus Volume Imaging and Analysis

Live tumor spheroids were stained with NucBlueTM Live ReadyProbesTM Reagent (Hoechst 33342, Thermofisher, #R37605) and fluorescent images were acquired using an Olympus FLUOVIEW FV3000 confocal microscope and 30X/1.05 NA silicon oil-immersion objective lens (UPLSAPO) with a step size of 0.71 μ m. Altogether, 51 nuclei were measured for the control condition and 27 nuclei for the osmotic shock conditions. Nuclei were selected randomly in the spheroids. Analysis: Z-stack Olympus (.oir) files were imported into ImageJ, where individual nuclei were cropped. (40) Image stacks (.tiff) were further analyzed in MATLAB using the 'isosurface' function and using the function 'boundary' to create a 3D ellipsoid mesh. The radii of the spheroids along the x, y, and z dimensions was used to calculate the volume using the equation $V = \frac{4}{3}\pi xyz$.

G. Cell Density Imaging and Analysis

Images were acquired with the Olympus FLUOVIEW FV3000 and 30X/1.05 NA objective lens. Three locations were randomly selected per spheroid and cells within the area were manually counted using ImageJ. The density was calculated by dividing the number of cells by the area of the image. Since image areas differed based on optimization, the density was normalized to an

area of $100 \times 100 \ \mu m^2$. 5 independent experiments were completed with a total of 15 images per condition.

H. Atomic Force Microscopy

A JPK NanoWizard 4a Atomic Force Microscope was employed in force contact mode to generate Young's moduli maps of live spheroids. To probe the cells, a CP-qp-CONT-Au sphere tip (Nanoandmore) with a diameter range of 3 - 5.5 μm was used. Measurements were performed using a 2 μm force distance, extend speed of 2.0 μm/s, and relative setpoint of 2.0 nN. Three 10 x 10 μm force maps with a step size of 1 μm/pixel were generated per spheroid. A total of 6 spheroids per condition were acquired. To extract the Young's modulus, force curves were fit to the Hertz model using the JPK Data Processing Software and following equation:

$$F = \frac{4}{3} \cdot \frac{E}{1 - \theta^2} \cdot \sqrt{r} \cdot \delta^{\frac{3}{2}}$$

Eq. 1

where δ is the measured indentation of the sample, E is the Young's modulus, ϑ is the Poisson's ratio, assumed to be 0.5, and r is tip radius of curvature, assumed to be approximately 5 μ m.

I. E-cadherin Staining Assay

Polyacrylamide gels with a 1.1 kPa shear modulus (G') were prepared as described previously. Tumor spheroids formed in a low attachment plate with 1,500 cells/well were seeded onto the gels. Four hours after transfer to polyacrylamide gels, medium was changed to a hypertonic (1000 mM sucrose) or hypotonic (25% media + 75% dH2O) solution for 5 or 30 minutes. For recovery experiments, hypertonic and hypotonic conditions were replenished with isotonic medium for same duration as the shock (either 5 or 30 minutes). Control spheroids in

isotonic medium were also prepared. Spheroids were subsequently fixed using 4% formaldehyde for 15 minutes at room temperature. Cells were rinsed three times in 1X PBS for 5 minutes each. A blocking buffer was prepared by mixing 0.5 ml normal goat serum (Cell Signaling, #5425), 0.5 ml 20X PBS, 9.0 ml dH2O, and 30 µl TritonTM X-100. 1 mL of the blocking buffer was added to the dishes for 1 hour. E-cadherin Rabbit mAb Alexa Fluor® 488 conjugate antibody (Cell Signaling, #3199) was added at 1:200 dilution and dishes were incubated overnight at 4°C. Cells were imaged using the Olympus FLUOVIEW FV3000. Analysis: ImageJ was used to convert the images to .PNG files and 16-bit. A threshold minimum was set to 20 counts to remove the background noise. The "analyze particles" function set to a size of 0 to 100 pixels². Circularity of 0 to 1.0 including holes was used to calculate the average clump size of E-cadherin. A total of 5 spheroids per condition were analyzed.

J. Statistical Analysis

For all experiments, a one-way ANOVA was used to compare groups. All statistics were performed using GraphPad Prism7. * \leq 0.05 ** \leq 0.01, *** \leq 0.001, **** \leq 0.0001.

II. Results and Discussion

Measuring Nucleus Volume in Tumor Spheroids

First, we explored the consequences of water transport on spheroids and nucleus morphology. To understand the timeframe over which morphology changes occur due to osmotic shock, we captured consecutive images every 5 seconds. We observed an increase in tumor spheroid surface area following a hypotonic shock and a decrease in tumor spheroid surface area following a hypertonic shock, with distinct morphological differences appearing within the first 5 minutes of shock (**Fig. 1, supplementary movie 1, 2**). Based on these observations, we

hypothesized that nucleus volume would also be affected as early as 5 minutes after the osmotic shock.

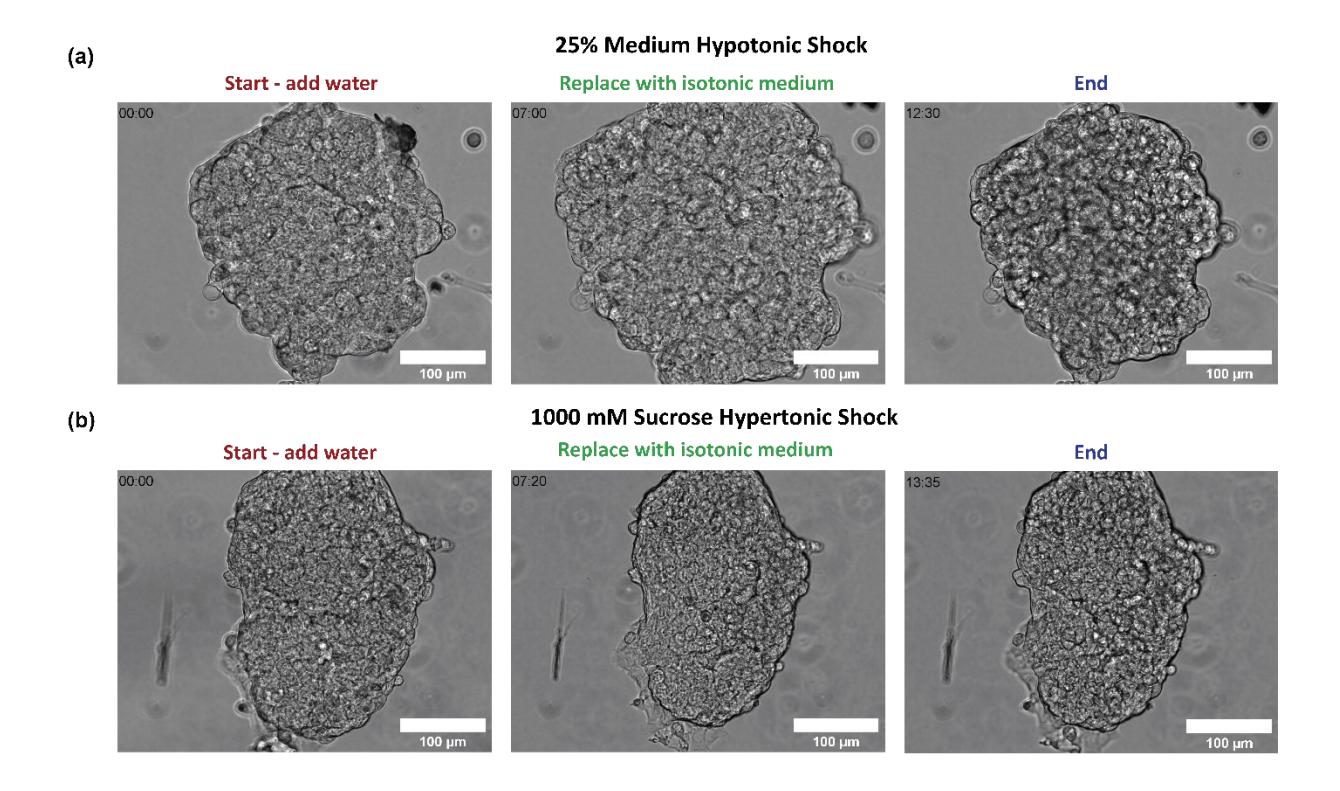


Figure 1 Timeframe of changes in spheroid morphology due to osmotic shock

(a) A representative image from movie (**supplementary video 1**) shows whole spheroid morphology due to a hypotonic shock performed with 25% medium and 75% water. Spheroids appeared to increase tumor area at the 7-minute time frame and return to its original size following approximately 5 minutes of replacement with isotonic medium. (b) A representative image from movie (**supplementary video 2**) shows the effects of whole spheroids morphology due to a hypertonic shock performed with 1000 mM sucrose in medium. Spheroids decreased tumor area at the 7:20 minute time frame and returned approximately 6 minutes after exposure to isotonic medium to its original size.

To quantify nucleus volume, three cells were randomly selected per spheroid, as indicated by the 'x' marks on the example (**Fig. 2 a**). While previous research has identified larger cell volumes at the periphery compared to the core (41), in the spheroids tested here, we did not observe heterogeneity based on distance within the spheroid. We hypothesize this could be due to culture time, since Han et al., showed heterogeneity appeared on day 5, but here we quantified after 3 days

of culture. The number of replicates per condition was 9 spheroids except for the control condition which was 17 spheroids. For each nucleus, confocal stacks of DAPI fluorescent images were acquired (**Fig. 2 b**). We measured cell volume and mechanical properties approximately 5 minutes after incubation with either sucrose or water mixtures. Within this timeframe we did not observe regulatory volume increase (RVI) or regulatory volume decrease (RVD) taking place. (42, 43) It is possible that after an extended period, cells would return to their original state.

Here, we quantified nucleus volume based on DAPI fluorescence and applied an in-house constructed algorithm in MATLAB to identify nucleus x, y, and z dimensions and calculate volume (**Fig. 2 c**). In each of the following experiments, two hypotonic (25% medium and 50% medium) and two hypertonic (500 mM and 1000 mM sucrose) conditions were tested. 100% medium was used as the control. As reported in **fig. 2 d**, the average osmolalities (mOsm/kg H₂O) were 71 ± 0 (25% medium), 139 ± 1 (25% medium), 278 ± 2 (control), 846 ± 17 (500 mM sucrose), and 1427 ± 35 (1000 mM sucrose). To report the relationship between osmolality and nucleus volume, data was plotted on a logarithmic scale ($\log Y = \kappa \log x + \log \alpha$) where the slope κ refers to the exponent of the linear plot $Y = \alpha x^{\kappa}$. Osmolality (mOsm/kg H₂O) and nucleus volume (μ m³) were related by an inverse correlation, $\log_{10} Y = 4.08 - 0.41 * \log_{10} X$ ($r^2 = 0.80$) (**Fig. 2 e**). The non-linearity of the osmotic-nucleus relationship appears to be due to the nucleus reaching a minimum volume at hyperosmotic shocks.

Given the changes in both cell volume and spheroid volume observed in supplementary videos 1 and 2 as a result of osmotic shock, we hypothesized that osmotic stress would result in a cohesive spatial movement of cells. To analyze this effect, we quantified tumor cell density by manually counting the number of nuclei per area. As shown in **figs. 2 f** and **S1**, increased osmolality caused cells to become

more loosely packed. Our data, along with previous literature, suggests that nucleus volume and density are linked in spheroid models and this relationship can even develop intratumorally. (41, 44)

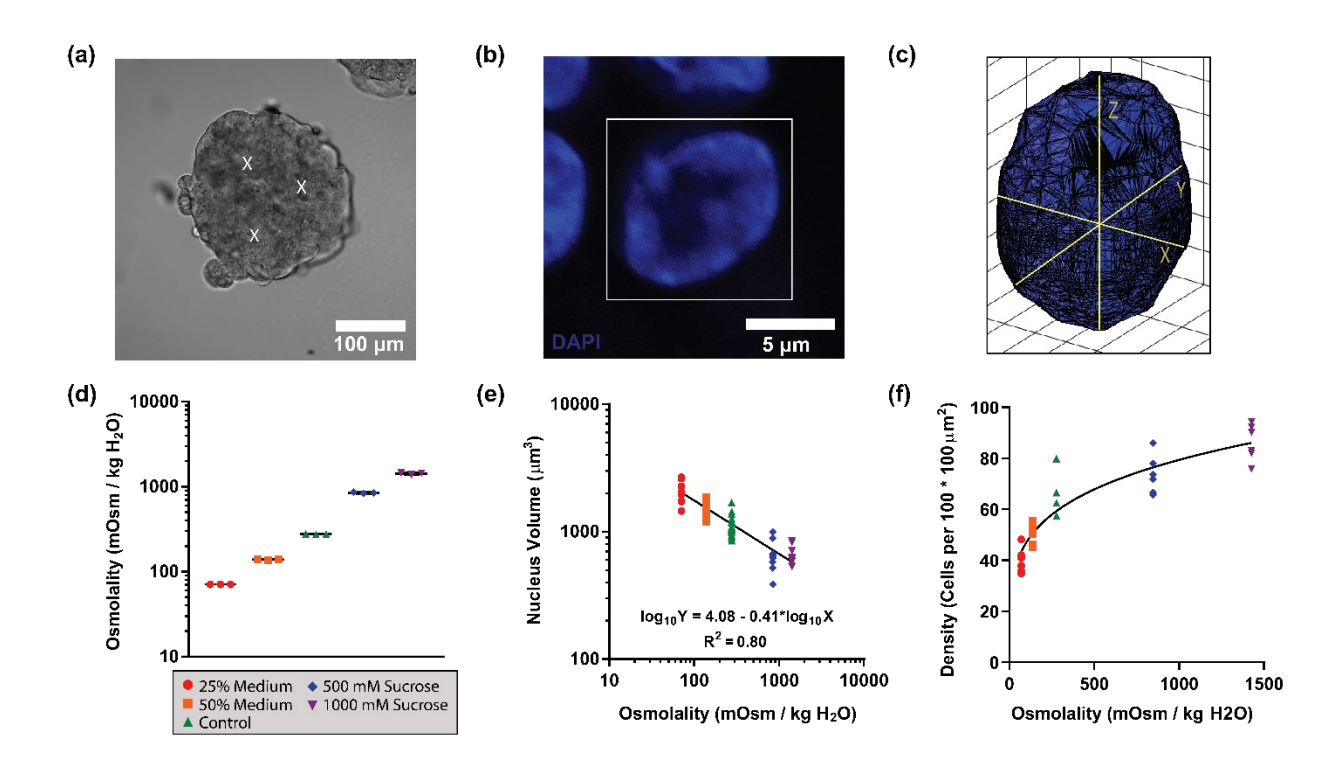


Figure 2 Relationship between osmolality and nucleus volume

(a) A representative image of a spheroid cultured using low-attachment spheroid dishes and transferred to a polyacrylamide gel coated with collagen. Spheroids became adhered to the surface after approximately 4 hours of incubation. Three nuclei at random locations within the spheroids were selected for volume analysis, as indicated by "X" symbols. Scale bar = $100 \mu m$. (b) Example fluorescent image of nucleus stained with DAPI. Scale bar = $5 \mu m$. (c) Representative image of nucleus volume calculated in MATLAB. (d) Osmolality of conditions acquired using an osmometer. Each data point represents one measurement and a total of 3 measurements were acquired. (e) Nucleus volume comparison between conditions: 25% medium + 75% dH2O (red circles), 50% medium + 50% dH2O (orange squares), control (green upward-triangles), 500μ mM sucrose (blue diamonds), 1000μ sucrose (purple downward-triangles). In total, 27 nuclei were measured for all conditions except for the control in which 51μ nuclei were measured. Each data point represents the average of 3 nuclei in a spheroid. (N = 9 spheroids for all conditions except the control where N = 17μ spheroids). (f) Density calculated as cells per 100μ x 100μ area at varying osmotic conditions. Each data point represents the average of 3 images captured within a single spheroid. N = 6μ spheroids per condition.

Link Between Osmolality and Young's Modulus

Next, we analyzed the effects of osmolality on the mechanical properties of spheroids using atomic force microscopy (AFM) (**Fig. 3 a**). We analyzed three regions per spheroid, each consisting of a 10 x 10 force map with a step size of 1 μ m as shown in **Fig. 3 b**. Using AFM, a correlation between osmolality (mOsm/kg H₂O) and Young's modulus (Pa) was observed. Young's modulus increased when water effluxed from the cell due to the compression of intracellular contents, and a concomitant decrease in Young's modulus was observed when water entered the cell. (26, 45) Osmolality and Young's modulus were related by $\log_{10} Y = -0.21 + 1.08 * \log_{10} X$ ($r^2 = 0.70$), which matched a prior power-law relationship between osmolality and Young's modulus obtained in single cells, where power κ was \sim 1. (45) (**Fig. 3 c**).

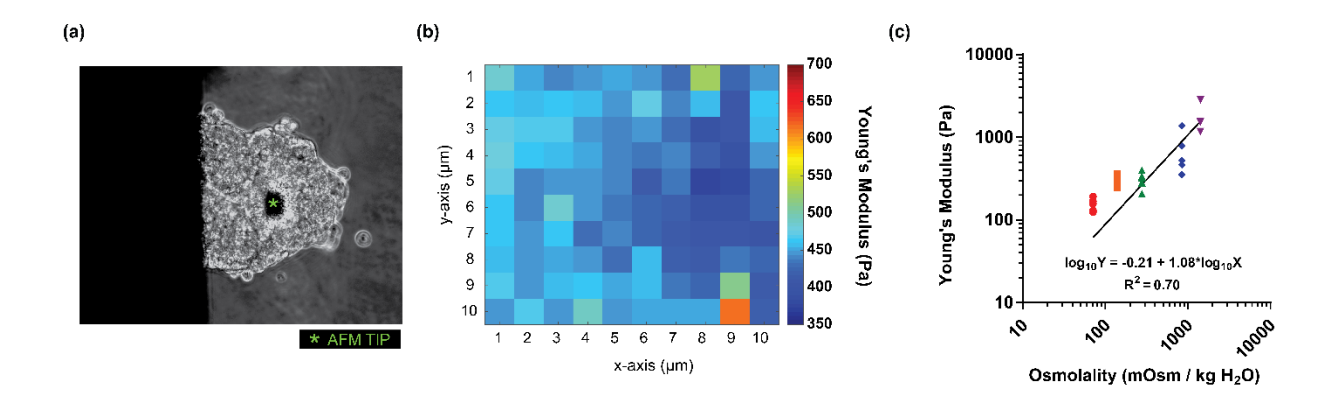


Figure 3 Osmolality and Young's Modulus

(a) Example brightfield image of a tumor spheroid adhered to a polyacrylamide gel coated with collagen. AFM probe location is represented by *. (b) Representative AFM map with 100 points total (10 x 10 μ m with 1 μ m step size). Color bar ranges from 350 Pa to 700 Pa. (c) Young's Modulus acquired for varying conditions: 25% medium (red circles), 50% medium (orange squares), control (green upward-triangles), 500 mM sucrose (blue diamonds), and 1000 mM sucrose (purple downward-triangles). Each data point represents the average Young's modulus of three 10 x 10 μ m maps (1 μ m step size) collected per spheroids. A total N = 5 spheroids per condition were analyzed.

Furthermore, when plotting nucleus volume versus Young's modulus (**Fig. S2**), we found a power of ~-2, which was nearly identical to a previous correlation obtained in single cells. (26) Overall, we found tumor spheroids resembled the morphology and mechanical response to water regulation observed in prior single cell measurements. (26, 45)

Tumor Spheroids can Recovery Volume, Density, Young's Modulus after Osmotic Shocks

Next, the reversibility of nucleus volume, density, and Young's modulus perturbations were tested. Understanding the effects of the microenvironment on the plasticity of morphological and phenotypic expression is of interest to study since cells experience versatile states including EMT and mesenchymal-epithelial-transition (MET) throughout cancer progression. Here, tumors were exposed to 5 minutes of 25% medium or 1000 mM sucrose and subsequently replenished with isotonic medium. There was a complete recovery of all three parameters demonstrating that osmotic effects are non-permanent. (**Fig. 4**). Our results corroborate previous findings showing, for example, that human colon carcinoma HT29 tumors cultured under 10 kPa of stress for 5 days using dextran relaxed back to the original volume. (46) Additionally, it was found that the temporal response of p27^{Kip1} expression reversed hours after volume, corresponding to the time of protein synthesis. (46) This is consistent with our results showing E-cadherin response acting on a longer time scale then morphology.

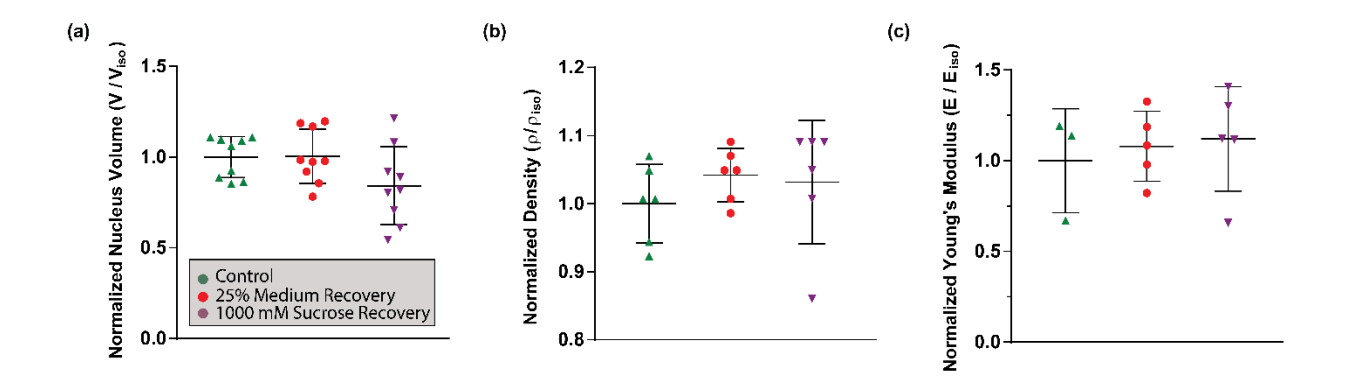


Figure 4 Nucleus volume, density, and Young's modulus after recovery

Measurements were acquired after a 5-minute osmotic shock and 5-minute replenishment with isotonic medium. Values are normalized to the average of the control group. A one-way ANOVA analysis revealed no significant difference between groups. Mean and standard deviation are displayed. (a) Recovery of nucleus volume. Each data point represents the average volume of 3 nuclei. A total of N=9 spheroids per

condition were acquired. (b) Recovery of density. Each data point represents the average of three images. A total of N=6 spheroids were analyzed. (c) Recovery of Young's modulus. Each data point represents the average of three $10 \times 10 \ \mu m$ maps with 100 points total. N=3 for control group and N=5 for osmotic shock groups.

Effect of Osmotic Shock on E-cadherin Expression

As shown in **supplementary movie 1 and 2**, morphology changes occurred within the first 5 minutes of osmotic shock; thus, we sought to identify whether concomitant molecular changes occurred. Spheroids were subjected to either 25% medium or 1000 mM sucrose for 5 or 30 minutes (**Fig. S3**). A control group with isotonic medium was also prepared. Spheroids were fixed and stained for E-cadherin using the protocol described in the methods section. To quantify E-cadherin aggregate size, we developed an algorithm in ImageJ. First, intensities of pixels less than 20 counts (background noise) were removed from the image. Next, we used the 'particle analysis' function to outline edges, fill holes, and to quantify the size of aggregates (**Fig. S4 a**). It was observed that E-cadherin was evenly distributed on the periphery of cells in the control spheroids (**Fig. S4 b**).

In our analysis to determine the timescale of E-cadherin effects, we found that a 30-minute osmotic shock caused increased E-cadherin protein aggregate size; in contrast to the negligible effects observed after a 5-minute osmotic shock. (Figs. 5, S5, S6). The delay likely signified that E-cadherin signaling acts on a timescale that is independent of changes in morphology. To evaluate the reversibility of molecular effects, spheroids were replenished with isotonic medium for a time equivalent to the initial shock (i.e., either 5 minutes or 30 minutes). Similar to prior mechanical and morphology recovery experiments, molecular E-cadherin distribution returned to baseline (Fig. 5). These observations support previous evidence on the strong influence of the tumor microenvironment and ability of cells to reverse their E-cadherin phenotype. (47) The specific role of E-cadherin protein aggregate size requires further analysis, but this preliminary work

emphasizes a potential relationship between E-cadherin aggregation, water volume regulation and mechanical properties.

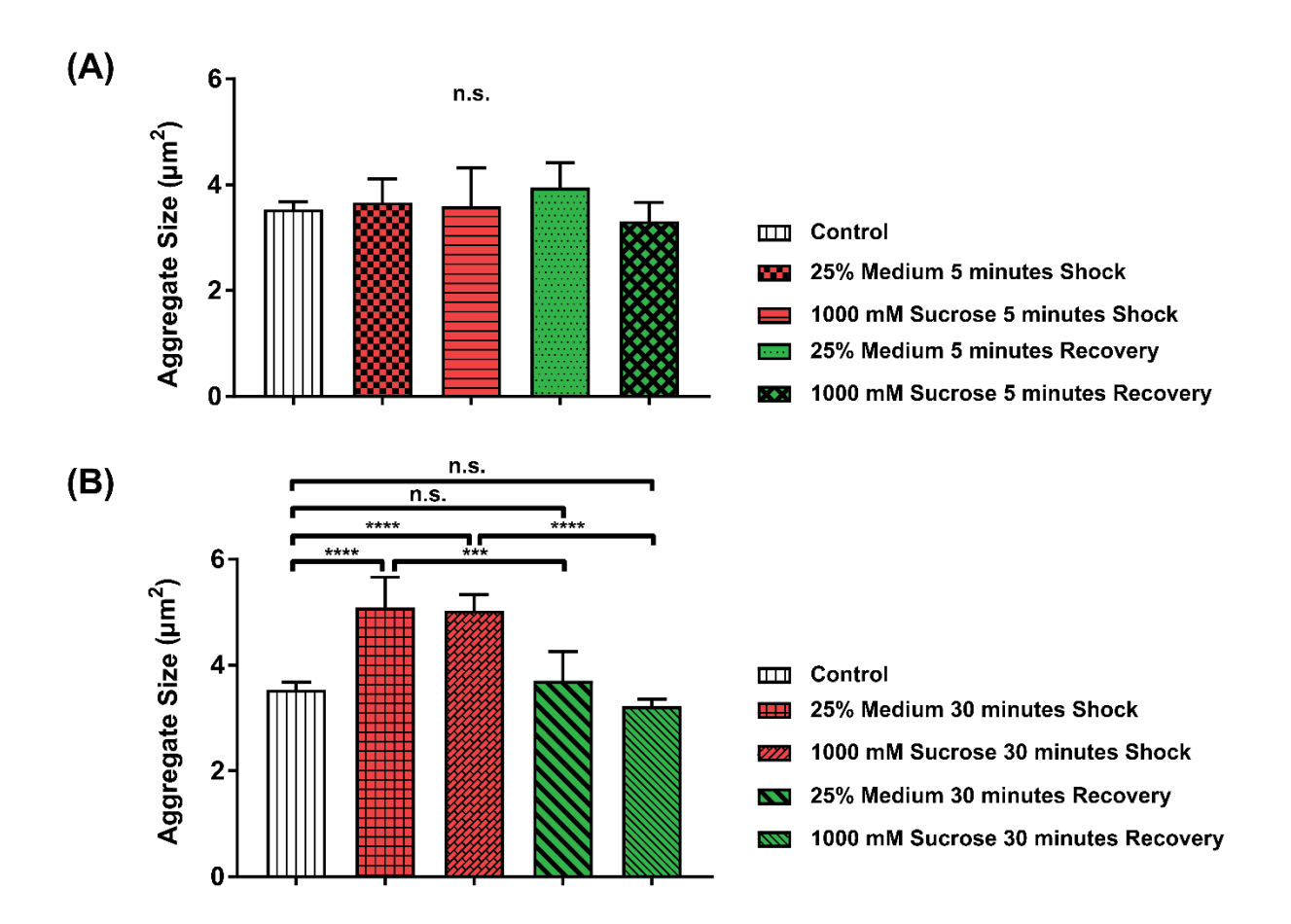


Figure 5 E-cadherin aggregate size analysis

Quantification of E-cadherin aggregate size (a) No change in aggregate size after 5 minutes of osmotic shock was observed. (b) A significant increase in aggregate size was found following 30 minutes of 25% medium and 1000 mM osmotic shocks. Aggregate size reduced to match the control condition after spheroids were re-immersed for 30 minutes in isotonic medium. A total of N = 5 spheroids were analyzed per condition. Statistics to analyze significant differences between groups were performed using a one-way ANOVA, where $p \le 0.05$ (*), $p \le 0.01$ (***), $p \le 0.001$ (****).

III. Conclusion

This study was guided by three major objectives: 1) to assess the changes in morphologic and mechanical responses due to water transport in tumor spheroids 2) to determine if osmotic shock drives permanent or reversible mechanical, morphology, and molecular variations; and 3)

to analyze changes in the distribution and expression of E-cadherin in response to osmotic shock and compare timescales of molecular effects with morphology. Our results demonstrated a non-linear osmotic-nuclear volume relationship as shown by the Ponder-Van't Hoff (48) plot (**Fig. S7**) which has also been shown in single cells. (26, 49) Subjecting cells to decreased osmolality (25% and 50% medium) results in an increased nucleus volume and decreased Young's modulus due to water influx, whereas an increased osmolality (500 mM sucrose and 1000 mM sucrose) results in a decreased nucleus volume and increased Young's modulus due to the efflux of water.

It remains unclear if an inverse volume-modulus correlation is universal across all cell types; but, it is likely that cells have unique properties based on their specific regulatory volume mechanisms and fraction of solid components in the cell. (26, 50–52) Wu et al. previously observed that the ratio between nuclear volume and cell volume was unique for different cell types (brain, breast, colorectal, lung, ovarian, pancreatic, prostate, melanoma). (53) For example, in the ovarian cancer cells used in the present study, the minimum nucleus volume following hyperosmotic shock was $659 \pm 110 \,\mu\text{m}^3$, corresponding to a solid fraction of the nucleus of ~60%. Guo et al. subjected bone marrow mesenchymal stem cells to hyperosmotic shock and found the solid fraction to be smaller, $\sim 27\%$ (minimum cell volume = $2053 \pm 30 \, \mu \text{m}^3$, control whole cell volume = $7646 \, \mu \text{m}^3$). (26) These differences in osmoregulation between cell types may be related to cell-cell adhesion interactions. For example, recently it was shown that cells that lack E-cadherin expression (MDA-MB-231) responded less to osmotic changes compared to cells with higher E-cadherin expression levels (non-malignant MCF-10A, malignant MCF-7 and MDCK). (50) Another factor driving the sensitivity to osmotic stress may be the fraction of osmotically unresponsive water i.e. the amount of water bound to intracellular constituents which is not displaced under osmotic stress. (27, 54, 55)

Our data suggest an important link between osmolality and the cell-cell adhesion marker, E-cadherin, which has not been studied previously. The interest to study E-cadherin was based off its prominent role in mediating numerous cell processes relevant to tumorigenesis including polarity, motility, and survival. (56, 57) Specifically, downregulated E-cadherin expression has been related to increased tumor aggressiveness, poor survival, perturbed barrier integrity, uncontrolled growth, increased aquaporin expression, and loss of contact inhibition. (58–64) Here, we quantified the size of fluorescently tagged E-cadherin and found that osmotic shock caused aggregation. Interestingly, spatial changes in E-cadherin distribution occurred on a longer timescale than the immediate morphological and mechanical response to osmotic shock. Ecadherin aggregation was only observed following 30 minutes of osmotic shock, but not after 5 minutes. Finally, we showed E-cadherin returned to its original state after reimmersion in isotonic medium. Future studies should assess the stability and maturity of these junctions after reassembly to confirm that E-cadherin completely recovers function. (65-67) In addition, a deeper understanding on the cytoplasmic localization of E-cadherin during aggregation, as well as the effect of osmotic shock on other molecules downstream of E-cadherin, is warranted.

In conclusion, osmoregulation is a critical process, which has been shown to be implicated in protein folding transport, chromatin condensation, proliferation, differentiation, and migration. (14, 15, 26, 68–71) This work highlighted an important role of water regulation in nucleus volume, Young's modulus, density, and E-cadherin expression. We found that all parameters could be reversed to its original state when provided with an isotonic condition after an osmotic shock. Given the extreme osmotic conditions tested in our experiments, we suspect that morphological, mechanical, and molecular effects in an *in vivo* state would also be reversible. Importantly, this work was performed in a single cell line (OVCAR5), thus we emphasize the importance of future

research to analyze other cell types. While we compare our 3D work to previous 2D work, given that we used an ovarian cancer cell line and Guo et al. used a bone marrow mesenchymal stem cell line (26), an important next step would be to perform similar experiments using the same cell line in both culture conditions. Additionally, a difference between 2D and 3D cultures can be the presence of extracellular matrix (ECM) proteins which may alter the response to osmotic shock based on how the osmolyte penetrates throughout the matrix. (72)

Finally, an interesting next step is to delve into the relationship between mechanical properties and the molecular events related to cell volume regulation. A classic model for cell volume regulation is the "pump and leak" mechanism in which the Na⁺ pump (Na+/K+ ATP-ase [NKA]) stabilizes cell volume (5, 73). Understanding whether targeting ion activity influences mechanical properties, or vice versa, could be a useful approach to gain control over behavioral properties such as the migration of cancer cells.

Particularly in ovarian cancer, it is important to understand how conditions like ascites or hyponatremia may influence mechanical, morphological, and molecular properties and should be accounted for when designing treatment strategies such as chemotherapy or peritoneal drainage. (35, 74, 75) Moreover, in the clinic, quantifying osmolality in various fluids relevant to disease states (*e.g.* plasma, peritoneal cavity, urine, etc.) will be helpful to guide in vitro experiments.

Author Contributions

Christina Conrad: Conceptualization, methodology, data curation, writing. Jessica Conway: Data curation and reviewing. William J. Polacheck: Supervision, reviewing, and editing. Imran Rizvi: Supervision, reviewing, and editing. Giuliano Scarcelli: Conceptualization, supervision, reviewing, and editing.

Conflicts of interest

There are no conflicts to declare.

Acknowledgements

We acknowledge the BioWorkshop core facility in the Fischell Department of Bioengineering at the University of Maryland, College Park for assistance with AFM and confocal imaging. This work was supported in part by the National Institutes of Health (R01HD095520, R00CA175292) and the National Science Foundation (CMMI 1929412, DBI 1942003), North Carolina Translational and Clinical Sciences Institute (NCTraCS), supported by the National Center for Advancing Translational Sciences (NCATS), (UL1TR002489) and UNC-NC State Joint BME Department Start-up Fund (WJP and IR).

References:

- 1. Lang, F., G.L. Busch, M. Ritter, H. Völkl, S. Waldegger, E. Gulbins, and D. Häussinger. 1998. Functional Significance of Cell Volume Regulatory Mechanisms. *Physiol. Rev.* 78:247–306.
- 2. Delpire, E., and K.B. Gagnon. 2018. Water Homeostasis and Cell Volume Maintenance and Regulation. *Curr. Top. Membr.* 81:3–52.
- 3. Brinkman, J., and s Sharma. 2018. Physiology, Body Fluids. .
- 4. Model, M.A. 2018. Methods for cell volume measurement. *Cytom. Part A.* 93:281–296.
- 5. Kay, A.R. 2017. How Cells Can Control Their Size by Pumping Ions . *Front. Cell Dev. Biol.* . 5:41.
- 6. Yancey, P.H. 2005. Organic osmolytes as compatible, metabolic and counteracting cytoprotectants in high osmolarity and other stresses. *J. Exp. Biol.* 208:2819 LP 2830.
- 7. Jentsch, T.J. 2016. VRACs and other ion channels and transporters in the regulation of cell volume and beyond. *Nat. Rev. Mol. Cell Biol.* 17:293–307.
- 8. Brown, D. 2017. The Discovery of Water Channels (Aquaporins). *Ann. Nutr. Metab.* 70(suppl 1):37–42.
- 9. Disalvo, E.A., O.A. Pinto, M.F. Martini, A.M. Bouchet, A. Hollmann, and M.A. Frías. 2015. Functional role of water in membranes updated: A tribute to Träuble. *Biochim. Biophys. Acta Biomembr.* 1848:1552–1562.

- 10. Fischbarg, J., K.Y. Kuang, J.C. Vera, S. Arant, S.C. Silverstein, J. Loike, and O.M. Rosen. 1990. Glucose transporters serve as water channels. *Proc. Natl. Acad. Sci. U. S. A.* 87:3244–3247.
- 11. Alberts, B., A. (Alexander D.. Johnson, J. 1946-2014 Lewis, D. 1958- Morgan, M.C. Raff, K. Roberts, P. (Professor) Walter, J. Wilson, and T. 1943- Hunt. 2015. Molecular biology of the cell LK https://umaryland.on.worldcat.org/oclc/926585551. Sixth edition. New York, NY SE xxxiv, 1342, G1-G34, I1-I53, T1 pages: illustrations (chiefly color); 28 cm: Garland Science.
- 12. Kim, D.-H., B. Li, F. Si, J.M. Phillip, D. Wirtz, and S.X. Sun. 2015. Volume regulation and shape bifurcation in the cell nucleus. *J. Cell Sci.* 128:3375 LP 3385.
- 13. Miermont, A., S.W.L. Lee, G. Adriani, and R.D. Kamm. 2019. Quantitative screening of the effects of hyper-osmotic stress on cancer cells cultured in 2- or 3-dimensional settings. *Sci. Rep.* 9:13782.
- 14. Pu, W., J. Qiu, G.J. Riggins, and M.-O. Parat. 2020. Matrix protease production, epithelial-to-mesenchymal transition marker expression and invasion of glioblastoma cells in response to osmotic or hydrostatic pressure. *Sci. Rep.* 10:2634.
- 15. Lee, H., R. Stowers, and O. Chaudhuri. 2019. Volume expansion and TRPV4 activation regulate stem cell fate in three-dimensional microenvironments. *Nat. Commun.* 10:529.
- 16. Nader, G.P. de F., A. Williart, and M. Piel. 2021. Nuclear deformations, from signaling to perturbation and damage. *Curr. Opin. Cell Biol.* 72:137–145.
- 17. Zlotek-Zlotkiewicz, E., S. Monnier, G. Cappello, M. Le Berre, and M. Piel. 2015. Optical volume and mass measurements show that mammalian cells swell during mitosis. *J. Cell Biol.* 211:765–774.
- 18. Montel, F., M. Delarue, J. Elgeti, L. Malaquin, M. Basan, T. Risler, B. Cabane, D. Vignjevic, J. Prost, G. Cappello, and J.-F. Joanny. 2011. Stress Clamp Experiments on Multicellular Tumor Spheroids. *Phys. Rev. Lett.* 107:188102.
- 19. De Ieso, M.L., and A.J. Yool. 2018. Mechanisms of Aquaporin-Facilitated Cancer Invasion and Metastasis. *Front. Chem.* 6:135.
- 20. Yan, C., Y. Zhu, X. Zhang, X. Chen, W. Zheng, and J. Yang. 2014. Down-regulated aquaporin 5 inhibits proliferation and migration of human epithelial ovarian cancer 3AO cells. *J. Ovarian Res.* 7:78.
- 21. Morishita, K., K. Watanabe, and H. Ichijo. 2019. Cell volume regulation in cancer cell migration driven by osmotic water flow. *Cancer Sci.* 110:2337–2347.
- 22. Direito, I., A. Madeira, M.A. Brito, and G. Soveral. 2016. Aquaporin-5: from structure to function and dysfunction in cancer. *Cell. Mol. Life Sci. TA TT -*. 73:1623–1640.
- 23. Wang, J., N. Tanji, T. Kikugawa, M. Shudou, X. Song, and M. Yokoyama. 2007. Expression of aquaporin 3 in the human prostate. *Int. J. Urol.* 14:1088–1092.
- 24. Khan, S., C. Ricciardelli, and A.J. Yool. 2021. Targeting Aquaporins in Novel Therapies

- for Male and Female Breast and Reproductive Cancers. Cells . 10.
- 25. Xie, K., Y. Yang, and H. Jiang. 2018. Controlling Cellular Volume via Mechanical and Physical Properties of Substrate. *Biophys. J.* 114:675–687.
- 26. Guo, M., A.F. Pegoraro, A. Mao, E.H. Zhou, P.R. Arany, Y. Han, D.T. Burnette, M.H. Jensen, K.E. Kasza, J.R. Moore, F.C. Mackintosh, J.J. Fredberg, D.J. Mooney, J. Lippincott-Schwartz, and D.A. Weitz. 2017. Cell volume change through water efflux impacts cell stiffness and stem cell fate. *PNAS*. 114:E8618-e8627.
- 27. Roffay, C., G. Molinard, K. Kim, M. Urbanska, V. Andrade, V. Barbarasa, P. Nowak, V. Mercier, J. García-Calvo, S. Matile, R. Loewith, A. Echard, J. Guck, M. Lenz, and A. Roux. 2021. Passive coupling of membrane tension and cell volume during active response of cells to osmosis. *Proc. Natl. Acad. Sci.* 118:e2103228118.
- 28. McManus, M.L., K.B. Churchwell, and K. Strange. 1995. Regulation of Cell Volume in Health and Disease. *N. Engl. J. Med.* 333:1260–1267.
- 29. Djamgoz, M.B.A. 2020. Hyponatremia and Cancer Progression: Possible Association with Sodium-Transporting Proteins. *Bioelectricity*. 2:14–20.
- 30. GD, S. 2005. Hyperosmolar hyperglycemic state. LK https://umaryland.on.worldcat.org/oclc/112042105. *Am. Fam. physician TA TT -*. 71:1723–1730.
- 31. Fortune, B., and A. Cardenas. 2017. Ascites, refractory ascites and hyponatremia in cirrhosis. *Gastroenterol. Rep.* 5:104–112.
- 32. Seri, I., R. Ramanathan, and J.R. Evans. 2005. Chapter 30 Acid-Base, Fluid, and Electrolyte Management. In: Taeusch HW, RA Ballard, CABT-AD of the N (Eighth E Gleason, editors. . Philadelphia: W.B. Saunders. pp. 372–397.
- 33. Berardi, R., M. Torniai, E. Lenci, F. Pecci, F. Morgese, and S. Rinaldi. 2019. Electrolyte disorders in cancer patients: a systematic review. *J. Cancer Metastasis Treat.* 5:79.
- 34. Kipps, E., D.S.P. Tan, and S.B. Kaye. 2013. Meeting the challenge of ascites in ovarian cancer: new avenues for therapy and research. *Nat. Rev. Cancer*. 13:273–282.
- 35. Gupta, S., M.C. Tio, E.D. Gutowski, M.S. Stecker, A. Verma, S.S. Motwani, D.B. Mount, G.M. McMahon, and S.S. Waikar. 2020. Incidence of Hyponatremia in Patients With Indwelling Peritoneal Catheters for Drainage of Malignant Ascites. *JAMA Netw. Open.* 3:e2017859–e2017859.
- 36. Meng, W., and M. Takeichi. 2009. Adherens junction: molecular architecture and regulation. *Cold Spring Harb. Perspect. Biol.* 1:a002899–a002899.
- 37. Wang, B., P. Qin, H. Zhao, T. Xia, J. Wang, L. Liu, L. Zhu, J. Xu, C. Huang, Y. Shi, and Y. Du. 2016. Substrate stiffness orchestrates epithelial cellular heterogeneity with controlled proliferative pattern via E-cadherin/β-catenin mechanotransduction. *Acta Biomater*. 41:169–180.
- 38. Paszek, M.J., N. Zahir, K.R. Johnson, J.N. Lakins, G.I. Rozenberg, A. Gefen, C.A.

- Reinhart-King, S.S. Margulies, M. Dembo, D. Boettiger, D.A. Hammer, and V.M. Weaver. 2005. Tensional homeostasis and the malignant phenotype. *Cancer Cell*. 8:241–254.
- 39. Ingber, D.E. 2008. Can cancer be reversed by engineering the tumor microenvironment? *Semin. Cancer Biol.* 18:356–364.
- 40. Schindelin, J., I. Arganda-Carreras, E. Frise, V. Kaynig, M. Longair, T. Pietzsch, S. Preibisch, C. Rueden, S. Saalfeld, B. Schmid, J.-Y. Tinevez, D.J. White, V. Hartenstein, K. Eliceiri, P. Tomancak, and A. Cardona. 2012. Fiji: an open-source platform for biological-image analysis. *Nat. Methods*. 9:676.
- 41. Han, Y.L., A.F. Pegoraro, H. Li, K. Li, Y. Yuan, G. Xu, Z. Gu, J. Sun, Y. Hao, S.K. Gupta, Y. Li, W. Tang, H. Kang, L. Teng, J.J. Fredberg, and M. Guo. 2019. Cell swelling, softening and invasion in a three-dimensional breast cancer model. *Nat. Phys.*
- 42. Okada, Y., E. Maeno, T. Shimizu, K. Dezaki, J. Wang, and S. Morishima. 2001. Receptor-mediated control of regulatory volume decrease (RVD) and apoptotic volume decrease (AVD). *J. Physiol.* 532:3–16.
- 43. Hoffmann, E.K., I.H. Lambert, and S.F. Pedersen. 2009. Physiology of Cell Volume Regulation in Vertebrates. *Physiol. Rev.* 89:193–277.
- 44. Grosser, S., J. Lippoldt, L. Oswald, M. Merkel, D.M. Sussman, F. Renner, P. Gottheil, E.W. Morawetz, T. Fuhs, X. Xie, S. Pawlizak, A.W. Fritsch, B. Wolf, L.-C. Horn, S. Briest, B. Aktas, M.L. Manning, and J.A. Käs. 2021. Cell and Nucleus Shape as an Indicator of Tissue Fluidity in Carcinoma. *Phys. Rev. X.* 11:11033.
- 45. Scarcelli, G., W.J. Polacheck, H.T. Nia, K. Patel, A.J. Grodzinsky, R.D. Kamm, and S.H. Yun. 2015. Noncontact three-dimensional mapping of intracellular hydro-mechanical properties by Brillouin microscopy. *Nat Methods*. 12:1132–1134.
- 46. Delarue, M., F. Montel, D. Vignjevic, J. Prost, J.-F. Joanny, and G. Cappello. 2014. Compressive Stress Inhibits Proliferation in Tumor Spheroids through a Volume Limitation. *Biophys. J.* 107:1821–1828.
- 47. Mohamet, L., K. Hawkins, and C.M. Ward. 2011. Loss of Function of E-Cadherin in Embryonic Stem Cells and the Relevance to Models of Tumorigenesis. *J. Oncol.* 2011:352616.
- 48. Ponder, E. 1948. Hemolysis and related phenomena. Saunders.
- 49. Zhou, E.H., X. Trepat, C.Y. Park, G. Lenormand, M.N. Oliver, S.M. Mijailovich, C. Hardin, D.A. Weitz, J.P. Butler, and J.J. Fredberg. 2009. Universal behavior of the osmotically compressed cell and its analogy to the colloidal glass transition. *PNAS*. 106:10632–10637.
- 50. Mohammed, D., C.Y. Park, J.J. Fredberg, and D.A. Weitz. 2021. Tumorigenic mesenchymal clusters are less sensitive to moderate osmotic stresses due to low amounts of junctional E-cadherin. *Sci. Rep.* 11:16279.
- 51. Pafundo, D.E., C.L. Alvarez, G. Krumschnabel, and P.J. Schwarzbaum. 2010. A volume

- regulatory response can be triggered by nucleosides in human erythrocytes, a perfect osmometer no longer. *J. Biol. Chem.* 285:6134–6144.
- 52. Finan, J.D., K.J. Chalut, A. Wax, and F. Guilak. 2008. Nonlinear Osmotic Properties of the Cell Nucleus. *Ann. Biomed. Eng.* 37:477.
- 53. Wu, Y., A.F. Pegoraro, D.A. Weitz, P. Janmey, and S.X. Sun. 2022. The correlation between cell and nucleus size is explained by an eukaryotic cell growth model. *PLOS Comput. Biol.* 18:e1009400.
- 54. Fullerton, G.D., K.M. Kanal, and I.L. Cameron. 2006. On the osmotically unresponsive water compartment in cells. *Cell Biol. Int.* 30:74–77.
- 55. Cameron, I.L., and G.D. Fullerton. 2014. Lack of appreciation of the role of osmotically unresponsive water in cell volume regulation. *Cell Biol. Int.* 38:610–614.
- 56. Venhuizen, J.-H., F.J.C. Jacobs, P.N. Span, and M.M. Zegers. 2020. P120 and E-cadherin: Double-edged swords in tumor metastasis. *Semin. Cancer Biol.* 60:107–120.
- 57. Yu, W., L. Yang, T. Li, and Y. Zhang. 2019. Cadherin Signaling in Cancer: Its Functions and Role as a Therapeutic Target. *Front. Oncol.* 9:989.
- 58. Mendonsa, A.M., T.-Y. Na, and B.M. Gumbiner. 2018. E-cadherin in contact inhibition and cancer. *Oncogene*. 37:4769–4780.
- 59. Rosso, M., B. Majem, L. Devis, L. Lapyckyj, M.J. Besso, M. Llauradó, M.F. Abascal, M.L. Matos, L. Lanau, J. Castellví, J.L. Sánchez, A. Pérez Benavente, A. Gil-Moreno, J. Reventós, A. Santamaria Margalef, M. Rigau, and M.H. Vazquez-Levin. 2017. E-cadherin: A determinant molecule associated with ovarian cancer progression, dissemination and aggressiveness. *PLoS One*. 12:e0184439–e0184439.
- 60. 2005. E-cadherin expression in ovarian carcinoma. *Nat. Clin. Pract. Oncol.* 2:6.
- 61. Loh, C.-Y., J.Y. Chai, T.F. Tang, W.F. Wong, G. Sethi, M.K. Shanmugam, P.P. Chong, and C.Y. Looi. 2019. The E-Cadherin and N-Cadherin Switch in Epithelial-to-Mesenchymal Transition: Signaling, Therapeutic Implications, and Challenges. *Cells*. 8:1118.
- 62. Lamouille, S., J. Xu, and R. Derynck. 2014. Molecular mechanisms of epithelial-mesenchymal transition. *Nat. Rev. Mol. Cell Biol.* 15:178–196.
- 63. Bordeleau, F., B.N. Mason, E.M. Lollis, M. Mazzola, M.R. Zanotelli, S. Somasegar, J.P. Califano, C. Montague, D.J. LaValley, and J. Huynh. 2017. Matrix stiffening promotes a tumor vasculature phenotype. *Proc. Natl. Acad. Sci.* 114:492–497.
- 64. Edamana, S., F.H. Login, S. Yamada, T.-H. Kwon, and L.N. Nejsum. 2021. Aquaporin water channels as regulators of cell-cell adhesion proteins. *Am. J. Physiol. Physiol.* 320:C771–C777.
- 65. de Beco, S., C. Gueudry, F. Amblard, and S. Coscoy. 2009. Endocytosis is required for E-cadherin redistribution at mature adherens junctions. *Proc. Natl. Acad. Sci.* 106:7010 LP 7015.

- 66. Indra, I., J. Choi, C.-S. Chen, R.B. Troyanovsky, L. Shapiro, B. Honig, and S.M. Troyanovsky. 2018. Spatial and temporal organization of cadherin in punctate adherens junctions. *Proc. Natl. Acad. Sci.* 115:E4406 LP-E4415.
- 67. Izumi, G., T. Sakisaka, T. Baba, S. Tanaka, K. Morimoto, and Y. Takai. 2004. Endocytosis of E-cadherin regulated by Rac and Cdc42 small G proteins through IQGAP1 and actin filaments. *J. Cell Biol.* 166:237–248.
- 68. Chen, X., C. Zhou, C. Yan, J. Ma, and W. Zheng. 2015. Hyperosmotic stress induces cisplatin sensitivity in ovarian cancer cells by stimulating aquaporin-5 expression. *Exp. Ther. Med.* 10:2055–2062.
- 69. Zhou, B., X. Lu, Y. Hao, and P. Yang. 2019. Real-Time Monitoring of the Regulatory Volume Decrease of Cancer Cells: A Model for the Evaluation of Cell Migration. *Anal. Chem.* 91:8078–8084.
- 70. Moeendarbary, E., L. Valon, M. Fritzsche, A.R. Harris, D.A. Moulding, A.J. Thrasher, E. Stride, L. Mahadevan, and G.T. Charras. 2013. The cytoplasm of living cells behaves as a poroelastic material. *Nat. Mater.* 12:253.
- 71. Stroka, K.M., H. Jiang, S.-H. Chen, Z. Tong, D. Wirtz, S.X. Sun, and K. Konstantopoulos. 2014. Water Permeation Drives Tumor Cell Migration in Confined Microenvironments. *Cell*. 157:611–623.
- 72. Dolega, M.E., S. Monnier, B. Brunel, J.-F. Joanny, P. Recho, and G. Cappello. 2021. Extracellular matrix in multicellular aggregates acts as a pressure sensor controlling cell proliferation and motility. *Elife*. 10:e63258.
- 73. TOSTESON, D.C., and J.F. HOFFMAN. 1960. Regulation of cell volume by active cation transport in high and low potassium sheep red cells. *J. Gen. Physiol.* 44:169–194.
- 74. Gupta, S., G.M. McMahon, S.S. Motwani, D.B. Mount, and S.S. Waikar. 2020. "Pleurex Desalination" in Malignancy-related Ascites: A Novel Mechanism of Hyponatremia. *Am. J. Clin. Oncol.* 43:14–19.
- 75. Yokoyama, Y., T. Shigeto, M. Futagami, and H. Mizunuma. 2005. Syndrome of inappropriate secretion of anti-diuretic hormone following carboplatin-paclitaxel administration in a patient with recurrent ovarian cancer. *Eur. J. Gynaecol. Oncol.* 26:531–532.

Supplementary Figures:

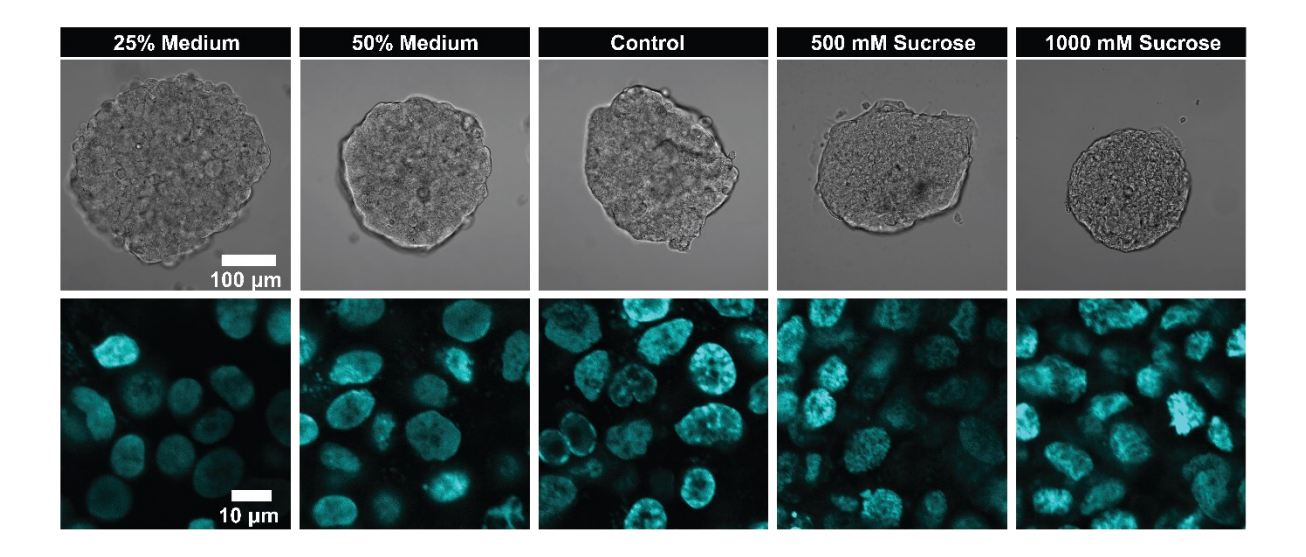


Figure S1 Effect of osmotic shock on tumor cell density

(Top) Brightfield images of tumor spheroids (scale bar = $100 \, \mu m$) (bottom) DAPI stained images (scale bar = $10 \, \mu m$) at varying osmotic conditions: 25% medium (red circle), 50% medium (orange square), control (green upward-triangle), 500 mM sucrose (blue diamond), and 1000 mM sucrose (purple downward-triangle). Higher osmolality caused an increased density.

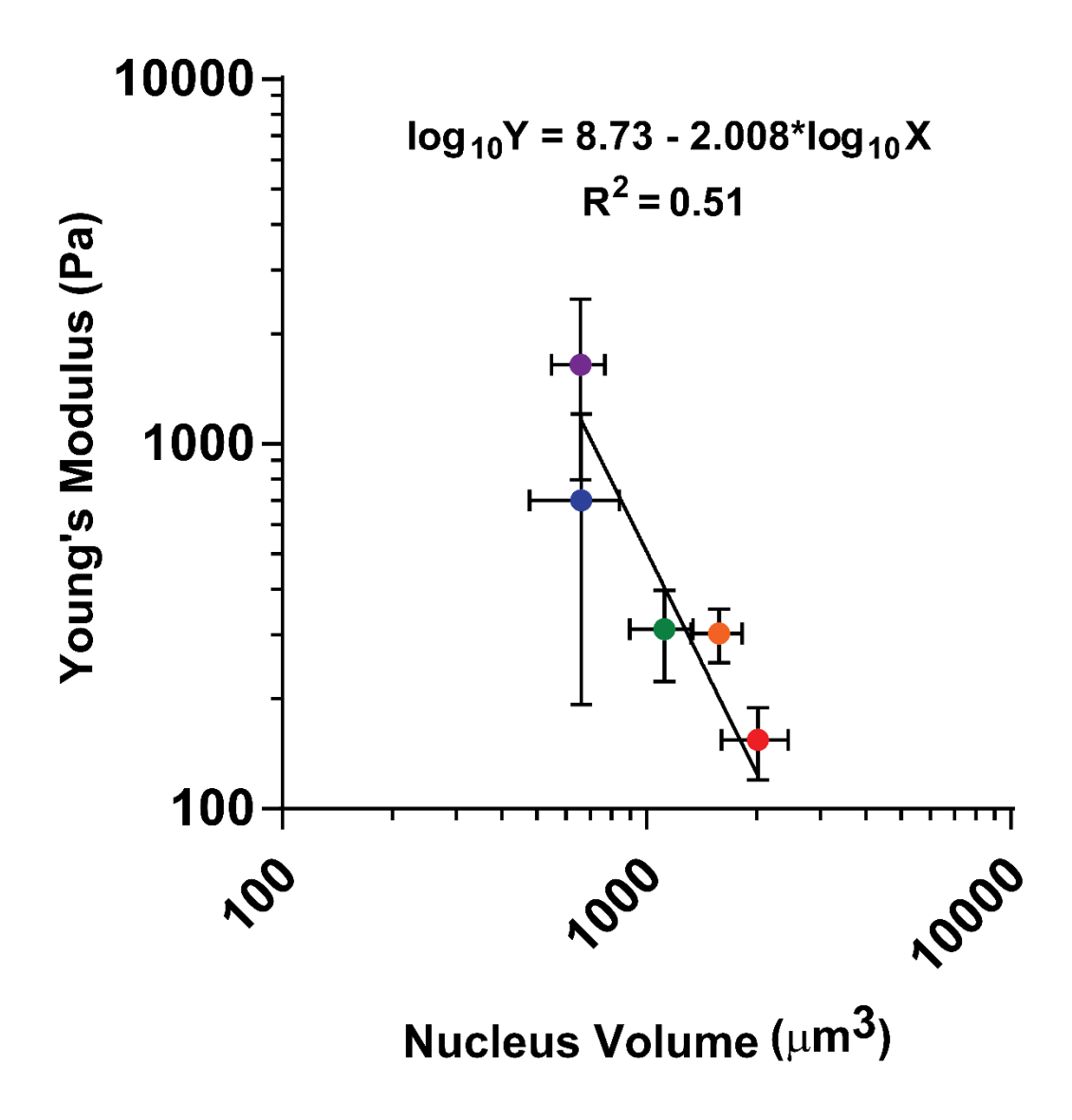


Figure S2 Correlation between nucleus volume and Young's Modulus

Nucleus volume from **fig. 2 e** and Young's modulus from **fig. 3 c** plotted. For nucleus volume, mean and standard deviation are displayed where each data point represents the average of 3 nuclei in a spheroid. A total N=9 spheroids were analyzed for all conditions except for the control condition where N=17. For Young's modulus, the mean and standard deviation are plotted where each data point represents the average Young's modulus of three $10 \times 10 \,\mu m$ maps ($1 \,\mu m$ step size) collected per spheroids. A total N=5 spheroids per condition were analyzed. Colors of data points refer to the varying osmotic conditions: 25% medium (red), 50% medium (orange), control (green), $500 \,m M$ sucrose (blue), and $1000 \,m M$ sucrose (purple).

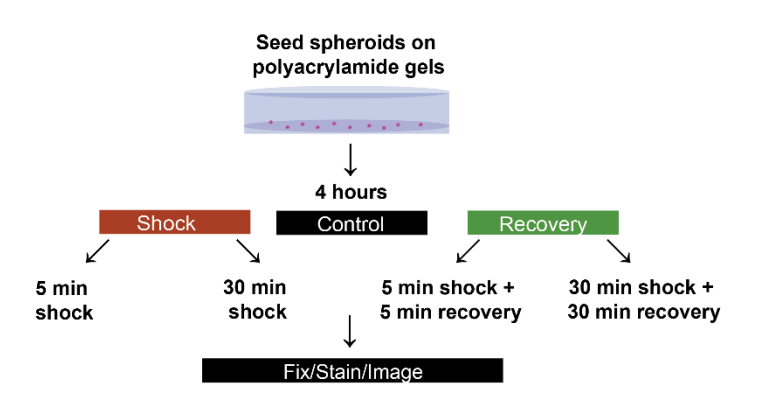


Figure S3 E-cadherin experiment design

E-cadherin staining protocol. Spheroids were immersed in 25% Medium or 1000 mM sucrose osmotic shock conditions for 5 or 30 minutes. For recovery experiments, spheroids were replenished with isotonic medium for the equivalent duration of the original shock (5 or 30 minutes).

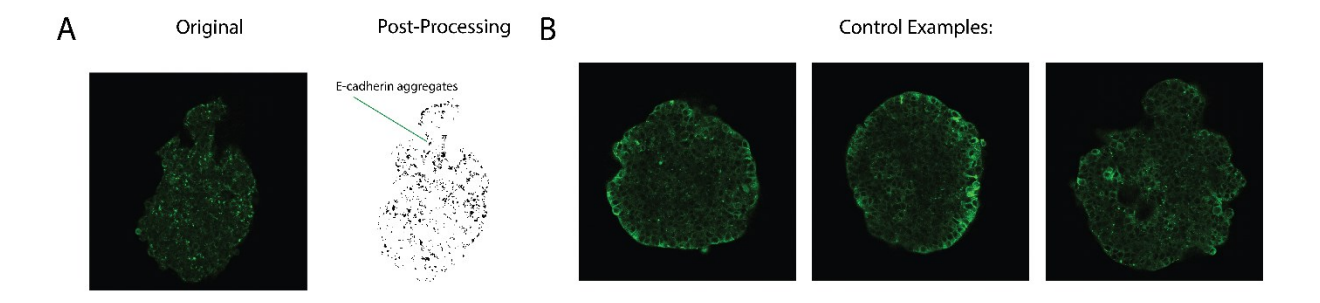


Figure S4 E-cadherin analysis method and control

(a) Example analysis of E-cadherin aggregate size performed in ImageJ. Low intensity background noise was eliminated using a threshold. Remaining high intensity pixels were analyzed using a particle analysis technique where pixels close in proximity were grouped together. The average size of an aggregate is reported. (b) Non-treated control spheroids showed E-cadherin on the periphery of cells. Scale bar = 100 μ m for all images.

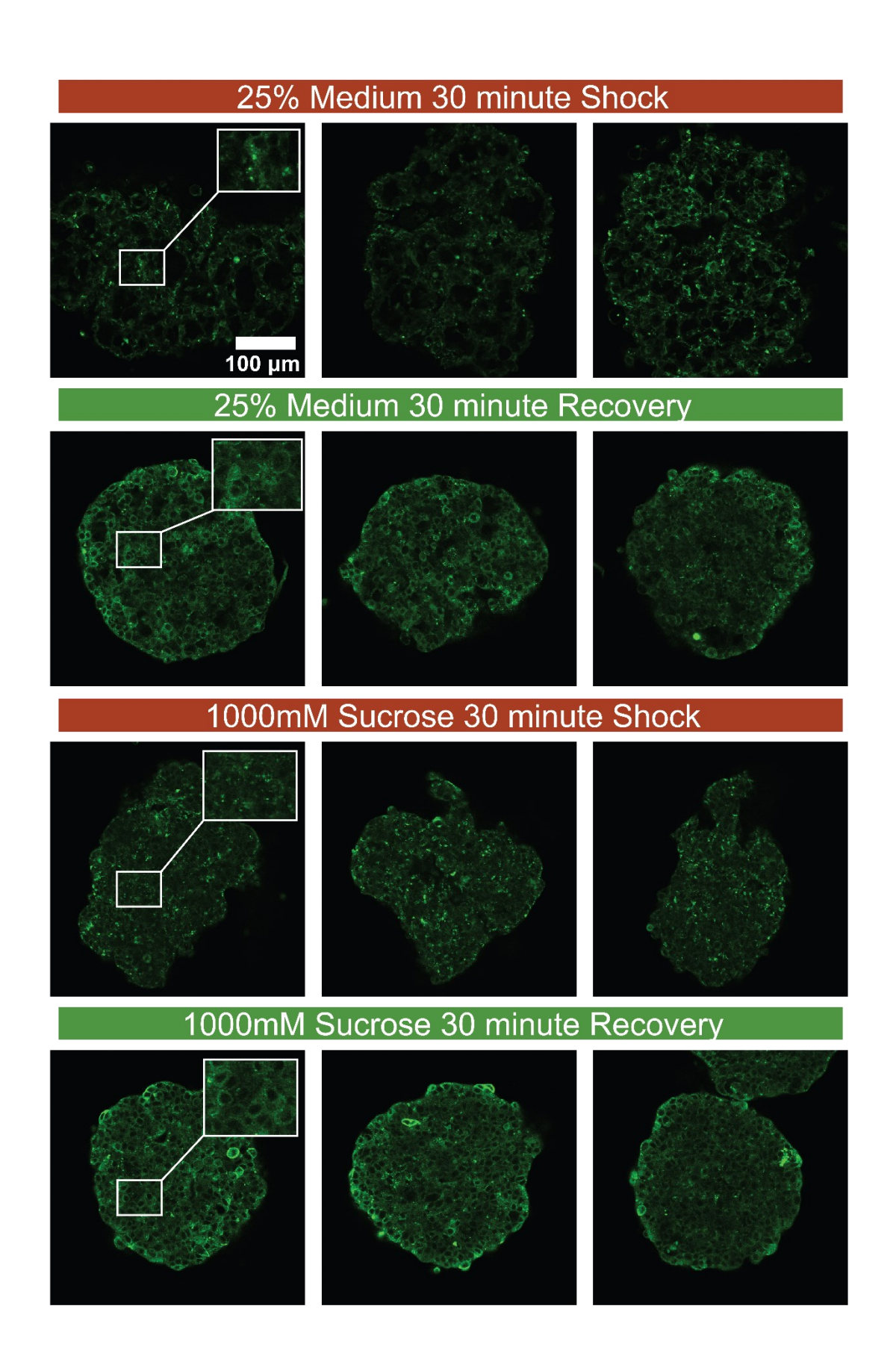


Figure S5 E-cadherin localization after 30 minutes of osmotic shocks

Representative images of E-cadherin expression after a 30-minute osmotic shock with 25% medium and 1000 mM sucrose. Recovery experiments were conducted by replenishing spheroids with isotonic medium after 30 minutes. E-cadherin aggregates appeared in both the 25% medium and 1000 mM sucrose following the 30-minute shock. E-cadherin recovered back to the original state when immersed in isotonic medium. Scale bar = $100 \, \mu m$ for all images.

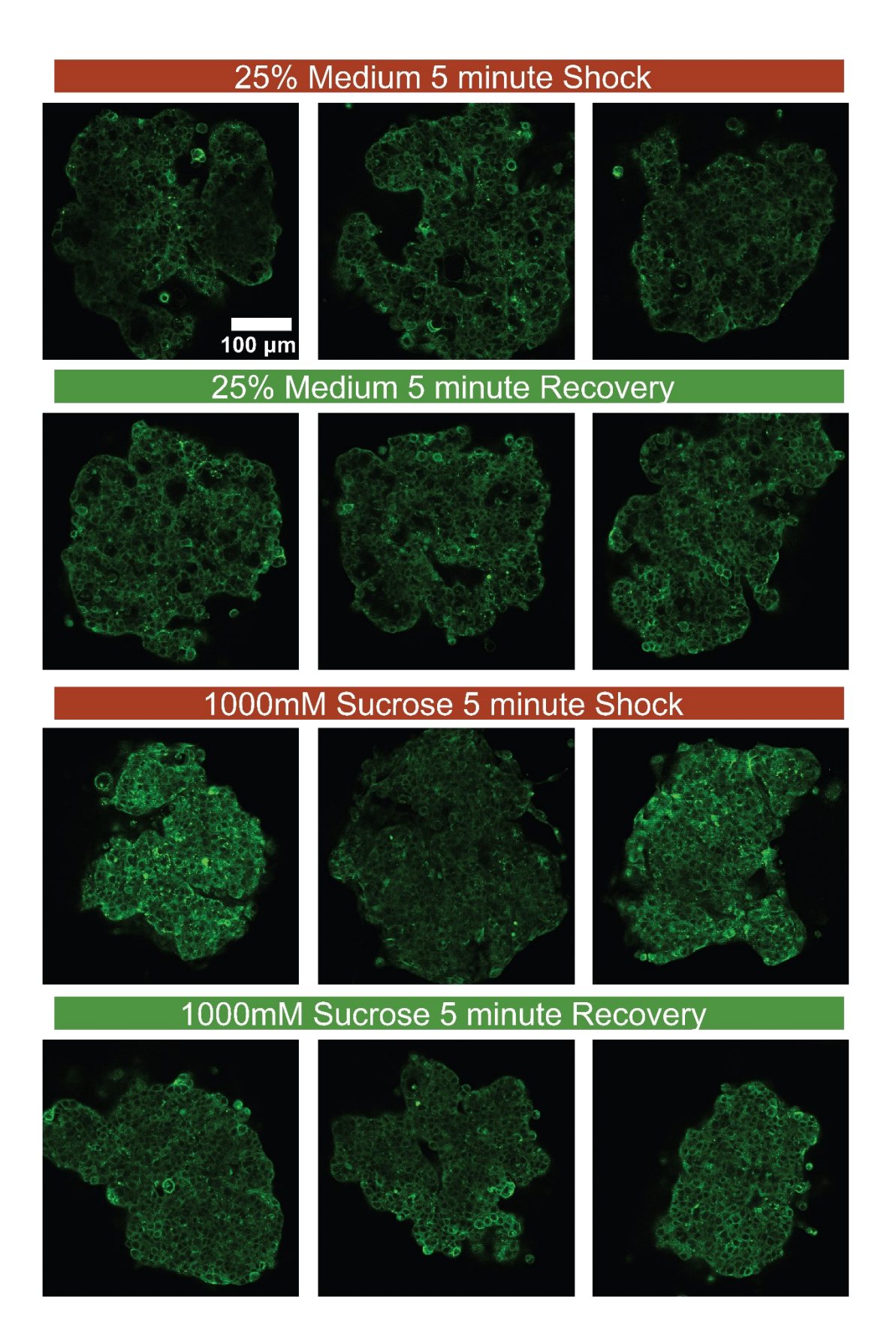


Figure S6 E-cadherin expression after 5 minutes of osmotic shock

Example images of E-cadherin expression after 5 minutes of 25% medium or 1000 mM sucrose osmotic shocks. Recovery experiments were performed by replenishing spheroids with 5 minutes of isotonic medium. No effects on E-cadherin aggregate size was observed after 5 minutes of hypotonic and hypertonic shocks. Scale bar = $100 \mu m$ for all images.

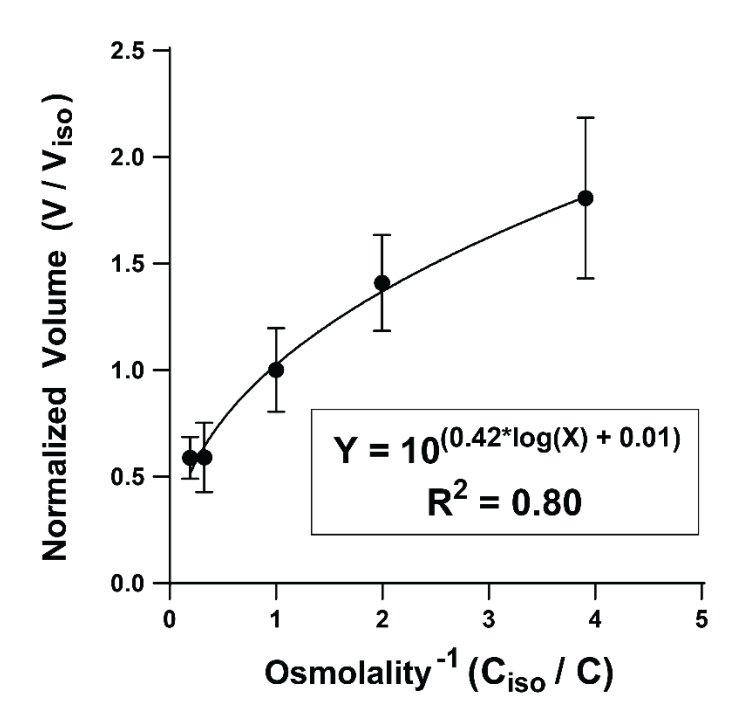


Figure S7 Ponder-Van't Hoff Relationship

A non-linear behavior is observed between osmolality and volume meaning the nucleus does not behave as an ideal osmometer. This observation can be explained by the physical limitations in the cell. A non-linear nuclear volume-osmolality relationship aligns with previous research. The y-intercept of the hyper-osmotic region (calculate by a line fit y = 0.3x+0.6) indicates that the solid fraction of the nucleus was 60% (V/Viso = 0.6)